

Computational Modeling and Simulation Examples in Bioengineering

Edited by
NENAD D. FILIPOVIC



IEEE Press Series in Biomedical Engineering
Metin Akay, Series Editor



IEEE Engineering in Medicine
and Biology Society, Sponsor

**IEEE PRESS**

WILEY

Table of Contents

[Cover](#)

[Series Page](#)

[Title Page](#)

[Copyright Page](#)

[Editor Biography](#)

[Author Biographies](#)

[Preface](#)

[1 Computational Modeling of Abdominal Aortic Aneurysms](#)

[1.1 Background](#)

[1.2 Clinical Trials for AAA](#)

[1.3 Computational Methods Applied for AAA](#)

[1.4 Experimental Testing to Determine Material Properties](#)

[1.5 Material Properties of the Aorta Wall](#)

[1.6 ILT Modeling](#)

[1.7 Finite Element Procedure and Fluid-Structure Interaction](#)

[1.8 Data Mining and Future Clinical Decision Support System](#)

[1.9 Conclusions](#)

[References](#)

[2 Modeling the Motion of Rigid and Deformable Objects in Fluid Flow](#)

[2.1 Introduction](#)

[2.2 Numerical Model](#)

[2.3 Results](#)

[2.4 Conclusion](#)

[References](#)

[3 Application of Computational Methods in Dentistry](#)

[3.1 Introduction](#)

[3.2 Finite Element Method in Dental Research](#)

[3.3 Examples of FEA in Clinical Research in Dentistry](#)

[References](#)

[4 Determining Young's Modulus of Elasticity of Cortical Bone from CT Scans](#)

[4.1 Introduction](#)

[4.2 Bone Structure](#)

[4.3 Young's Modulus of Elasticity of Bone Tissue](#)

[4.4 Tool for Calculating the Young's Modulus of Elasticity of Cortical Bone from CT Scans](#)

[4.5 Numerical Analysis of Femoral Bone Using Calculated Elasticity Modulus](#)

[4.6 Conclusion](#)

[Acknowledgements](#)

[References](#)

[5 Parametric Modeling of Blood Flow and Wall Interaction in Aortic Dissection](#)

[5.1 Introduction](#)

[5.2 Medical Background](#)

[5.3 Theoretical Background](#)

[5.4 Blood Flow in the Arteries](#)

[5.5 Numerical Simulations](#)

[5.6 Conclusions](#)

References

6 Application of AR Technology in Bioengineering

6.1 Introduction

6.2 Review of AR Technology

6.3 Marker-based AR Simple Application, Based on the OpenCV Framework

6.4 Marker-less AR Simple Application, Based on the OpenCV Framework

6.5 Conclusion

References

7 Augmented Reality Balance Physiotherapy in HOLOBALANCE Project

7.1 Introduction

7.2 Motivation

7.3 Holograms-Based Balance Physiotherapy

7.4 Mock-ups

7.5 Final Version

7.6 Biomechanical Model of Avatar Based on the Muscle Modeling

References

8 Modeling of the Human Heart - Ventricular Activation Sequence and ECG Measurement

8.1 Introduction

8.2 Materials and Methods

8.3 Determination of Stretches in the Material Local Coordinate System

8.4 Determination of Normal Stresses from Current Stretches

8.5 Results and Discussion

8.6 Conclusion

[Acknowledgements](#)

[References](#)

[9 Implementation of Medical Image Processing Algorithms on FPGA Using Xilinx System Generator](#)

[9.1 Brief Introduction to FPGA](#)

[9.2 Building a Simple Model Using XSG](#)

[9.3 Medical Image Processing Using XSG](#)

[9.4 Results and Discussion](#)

[9.5 Conclusions](#)

[Acknowledgments](#)

[References](#)

[Index](#)



[IEEE Press Series in Biomedical Engineering](#)

[End User License Agreement](#)

List of Tables

Chapter 2

[Table 2.1 Lattice structures - weight coefficients and vectors defining abs...](#)

Chapter 3

[Table 3.1 Mechanical properties of dental structures and restorative materi...](#)

[Table 3.2 Values of the material strength \(\$\sigma_{SM}\$ \) were adopted from lite...](#)

[Table 3.3 Maximum effective stress, maximum displacement, maximum tensile a...](#)

[Table 3.4 Material properties of each modeled structure.](#)

[Table 3.5 Overall FEA results.](#)

Chapter 4

[Table 4.1 Overview of empirical expression available in the literature.](#)

[Table 4.2 Elasticity modulus for cortical bones.](#)

[Table 4.3 Young's elasticity modulus of the cortical femoral bone.](#)

[Table 4.4 Material properties of the trabecular femoral bone.](#)

[Table 4.5 Description of the applied forces.](#)

[Table 4.6 Comparison of the calculated maximum stress values.](#)

[Table 4.7 Comparison of the calculated maximum displacement values.](#)

Chapter 7

[Table 7.1 Presents the list of phrases that the BPH uses and that provide t...](#)

Chapter 8

[Table 8.1 Parameters for the monodomain model with modified FitzHugh-Nagumo...](#)

Chapter 9

[Table 9.1 Xilinx Blockset library description \[1\].](#)

[Table 9.2 Supported Matlab and XSG versions.](#)

[Table 9.3 Post synthesis resource utilization summary.](#)

[Table 9.4 Post synthesis timing paths.](#)

List of Illustrations

Chapter 1

[Figure 1.1 \(a\) Cartoon schema. \(b\) Real laboratory model. Laboratory model c...](#)

[Figure 1.2 \(a\) Shear stress distribution. \(b\) Drag force distribution.](#)

[Figure 1.3 \(a\) Shear stress distribution. \(b\) Drag force distribution.](#)

[Figure 1.4 Description of clinical decision support system for AAA disease....](#)

[Figure 1.5 Geometrical parameters of AAA: "Length" is the parameter which de...](#)

[Figure 1.6 A typical in-flow waveform at the aorta entry. \$Q\$ is the volumetri...](#)

[Figure 1.7 Velocity field \(left panel\) and pressure distribution \(right pane...](#)

[Figure 1.8 Input velocity and output pressure profiles for the AAA on a stra...](#)

[Figure 1.9 Velocity magnitude field and von Mises wall stress distribution f...](#)

Chapter 2

[Figure 2.1 Diagram of variation of Dirac delta function depending on the dis...](#)

[Figure 2.2 Example 1 - Geometry of the fluid domain.](#)

[Figure 2.3 Example 1 - Fluid velocity field and current position of the sphe...](#)

[Figure 2.4 Example 1 - Change of shape over time of the spherical particle, ...](#)

[Figure 2.5 Example 1 - Change of shape over time of the spherical particle, ...](#)

[Figure 2.6 Example 1 - Change of shape over time of the spherical particle, ...](#)

[Figure 2.7 Example 1 - Fluid velocity field and current position of RBC - fi...](#)

[Figure 2.8 Example 1 - Fluid velocity field and current position of RBC - se...](#)

[Figure 2.9 Example 1 - Change of shape of RBC over time - first considered c...](#)

[Figure 2.10 Example 1 - Change of shape of RBC over time - second considered...](#)

[Figure 2.11 Example 2 - Geometry of the fluid domain.](#)

[Figure 2.12 Cross-section of a spherical particle during deformation and the...](#)

[Figure 2.13 Example 2 - Fluid velocity field and the current position of a s...](#)

[Figure 2.14 Example 2 - Velocity streamlines.](#)

[Figure 2.15 Example 2 - Comparison of the final shape of spherical particle ...](#)

[Figure 2.16 Example 2 - Variation of Taylor deformation index over time, for...](#)

[Figure 2.17 Example 2 - Variation of inclination angle over time, for differ...](#)

[Figure 2.18 Example 2 - Variation of inclination angle over time, for a rigi...](#)

[Figure 2.19 Example 2 - Variation of Taylor deformation index over time, for...](#)

[Figure 2.20 Example 2 - Variation of Taylor deformation index over time, for...](#)

[Figure 2.21 Example 2 - Deformation of the particle for \$G=0.1\$ for different ...](#)

[Figure 2.22 Example 2 - Variation of Taylor deformation index over time, for...](#)

[Figure 2.23 Example 2 - Deformation of the particle during restoration of in...](#)

[Figure 2.24 Example 2 - Variation of Taylor deformation index over time, \$\lambda...\$](#)

[Figure 2.25 Example 2 - Variation of Taylor deformation index over time, \$\lambda...\$](#)

[Figure 2.26 Example 2 - Variation of inclination angle over time, for differ...](#)

[Figure 2.27 Example 2 - Change of shape of RBC over time, for \$Ca = 0.1\$; soli...](#)

[Figure 2.28 Example 2 - Change of shape of RBC over time, for \$Ca = 0.5\$; soli...](#)

[Figure 2.29 Example 2 - Velocity streamlines for \$Ca = 0.1\$.](#)

[Figure 2.30 Example 2 - Velocity streamlines for \$Ca = 0.5\$.](#)

[Figure 2.31 Example 2 - Motion of rigid and deformable particle through the ...](#)

[Figure 2.32 Example 2 - Change of x component of particle velocity during si...](#)

[Figure 2.33 Example 2 - Change of y component of particle velocity during si...](#)

[Figure 2.34 Example 3 - Motion of rigid and deformable particle through the ...](#)

[Figure 2.35 Example 3 - Change of x component of particle velocity during si...](#)

[Figure 2.36 Example 3 - Change of y component of particle velocity during si...](#)

[Figure 2.37 Example 4 - Motion of rigid and deformable particle through the ...](#)

[Figure 2.38 Example 4 - Geometry of the three-dimensional artery with bifurc...](#)

[Figure 2.39 Example 4 - Fluid pressure field and initial position of RBC.](#)

[Figure 2.40 Example 4 - Simulation of motion of RBC through an artery with b...](#)

[Figure 2.41 Example 4 - Change of shape of RBC over time.](#)

Chapter 3

[Figure 3.1 \(a\). Model of complete lower jaw with all needed anatomical and h...](#)

[Figure 3.2 \(a\). Linear static occlusal load on tooth surface \(b\). Modeling o...](#)

[Figure 3.3 Muscles attachment areas, direction of forces, and constrains.](#)

[Figure 3.4 Schematic overview of the sequential steps performed in this stud...](#)

[Figure 3.5 Presentation of different structures in each tooth model.](#)

[Figure 3.6 Diagram of compressive displacement \(strain\) dependencies on comp...](#)

[Figure 3.7 Distribution of principal \(d-i\) and Von Mises stress \(a-c\) observ...](#)

[Figure 3.8 Distribution of principal stresses and Failure Indices in Model 1...](#)

[Figure 3.9 Distribution of principal stresses \(a-c, g-i,\) and corresponding ...](#)

[Figure 3.10 FEM procedures: \(a-c\) Considered models, \(d\) schematic view of t...](#)

[Figure 3.11 Goodman's diagram.](#)

[Figure 3.12 Three characteristic phases of fatigue crack growth \(region I - ...](#)

[Figure 3.13 FEA results for Model 1 under occlusal load of 100N, 150N and 200...](#)

[Figure 3.14 Developed shrinkage stresses for the considered restoration case...](#)

[Figure 3.15 FEA results for Model 2; \(a\) - \(i\) low-shrinkage stress cases, \(...](#)

[Figure 3.16 FEA results for Model 3; \(a\) - \(i\) low-shrinkage stress cases, \(...](#)

[Figure 3.17 Fatigue failure diagrams: \(a\), \(b\). Goodman's diagrams for Model ...](#)

Chapter 4

[Figure 4.1 Bone shapes.](#)

[Figure 4.2 Cortical and trabecular.](#)

[Figure 4.3 Comparison of four empirical expressions.](#)

[Figure 4.4 Algorithm for calculation of elasticity modulus.](#)

[Figure 4.5 A list of information contained in a CT scan.](#)

[Figure 4.6 Effect of threshold value on the segmentation of the femoral bone...](#)

[Figure 4.7 Printing of the calculated values.](#)

[Figure 4.8 Visual representation of the original image and segmented bone us...](#)

[Figure 4.9 Femoral body in the transverse plane before segmentation.](#)

[Figure 4.10 Femoral body in the transverse plane after segmentation.](#)

[Figure 4.11 Femoral bone model.](#)

[Figure 4.12 Applied boundary conditions for the numerical simulations.](#)

[Figure 4.13 Obtained stress distribution - case 1.](#)

[Figure 4.14 Obtained displacement distribution - case 1.](#)

[Figure 4.15 Obtained stress distribution - case 2.](#)

[Figure 4.16 Obtained displacement distribution - case 2.](#)

[Figure 4.17 Obtained stress distribution - case 3.](#)

[Figure 4.18 Obtained displacement distribution - case 3.](#)

[Figure 4.19 Correlation between Young's modulus of elasticity and calculated...](#)

[Figure 4.20 Correlation between Young's modulus of elasticity and calculated...](#)

Chapter 5

[Figure 5.1 Schematic representation of the cardiovascular system \[28\].](#)

[Figure 5.2 Anatomy of the aorta \[21\].](#)

[Figure 5.3 The structure of the wall of the main components of healthy elast...](#)

[Figure 5.4 CT scan shows the false and true lumen.](#)

[Figure 5.5 Classification of aortic dissection.](#)

[Figure 5.6 Coordinate definitions.](#)

[Figure 5.7 Schematic representation of a deformable body under the action of...](#)

[Figure 5.8 Schematic representation of the distorted axial velocity profile ...](#)

[Figure 5.9 Schematic representation of the velocity profile in bifurcation....](#)

[Figure 5.10 Geometric dimensions of the aorta.](#)

[Figure 5.11 Geometries of parametric models: \(a\) healthy aorta; \(b\) dissecte...](#)

[Figure 5.12 The time-dependent pulsatile waveform at the ascending aorta.](#)

[Figure 5.13 Example 1 - distribution of velocity \(a\) and pressure \(b\) throug...](#)

[Figure 5.14 Example 1 - distribution of shear stress on fluid domain \(a\) and...](#)

[Figure 5.15 Example 2 - distribution of velocity \(a\) and pressure \(b\) throug...](#)

[Figure 5.16 Example 2 - distribution of wall shear stress on fluid domain \(a...](#)

[Figure 5.17 Example 3 - distribution of velocity \(a\) and pressure \(b\) throug...](#)

[Figure 5.18 Example 3 - distribution of wall shear stress on fluid domain \(a...](#)

[Figure 5.19 Example 4 - distribution of velocity \(a\) and pressure \(b\) throug...](#)

[Figure 5.20 Example 4 - distribution of wall shear stress on fluid domain \(a...](#)

Chapter 6

[Figure 6.1 A simple example of augmented reality.](#)

[Figure 6.2 Schematic representation of AR monitor system.](#)

[Figure 6.3 Augmented reality application on mobile phone.](#)

[Figure 6.4 Schematic diagrams: SHDM device \(left\); VHDM device \(right\).](#)

[Figure 6.5 Schematic representation - the fundamental principle of AR system...](#)

[Figure 6.6 Dome and arrow during the suturing task to guide the trainee in t...](#)

[Figure 6.7 Schematic representation of the flow of an AR-based biomedical en...](#)

[Figure 6.8 Some examples of ArUco markers.](#)

[Figure 6.9 Example of ArUco marker.](#)

[Figure 6.10 ArUco markers on the wall - preparation AR scene.](#)

[Figure 6.11 An example of using ArUco marker - AR images on a real wall.](#)

[Figure 6.12 ArUco markers - biomedical application.](#)

[Figure 6.13 Matching results by using cross-checks filter.](#)

[Figure 6.14 Visualization of matches that were refined using homography matr...](#)

[Figure 6.15 Visualization of matches that were refined using refinement homo...](#)

[Figure 6.16 Examples of calibration images.](#)

[Figure 6.17 AR result with wrong calibration parameters \(left\); with good ca...](#)

[Figure 6.18 Accurate tracking of liver tumors for augmented reality in robot...](#)

Chapter 7

[Figure 7.1 Balance physiotherapy mock-up motion capture and display devices....](#)

[Figure 7.2 Balance physiotherapy hologram using Meta 2 and Kinect 2 for stan...](#)

[Figure 7.3 First versions of avatars used with Meta 2. Realistic Female Virt...](#)

[Figure 7.4 HoloLens Virtual Coach \(VC\).](#)

[Figure 7.5 Virtual Coach initial standing position \(a\) and direction indicat...](#)

[Figure 7.6 Gazing pointers. \(a\) White pointer when gazing out of VC and \(b\) ...](#)

[Figure 7.7 Hand gesture. Interacting with VC. VC demonstrates exercise after...](#)

[Figure 7.8 Voice gesture. Interacting with VC. VC demonstrates exercise afte...](#)

[Figure 7.9 HoloBox schematic setup.](#)

[Figure 7.10 Test version - demonstrates exercise.](#)

[Figure 7.11 Conceptual architecture of the interfacing modules with the MCWS...](#)

[Figure 7.12 Avatars.](#)

[Figure 7.13 Virtual Coach Demo mode with controls.](#)

[Figure 7.14 Sitting exercise - yaw.](#)

[Figure 7.15 Sitting exercise - pitch.](#)

[Figure 7.16 Sitting exercise - bend over.](#)

[Figure 7.17 Standing exercise - maintain balance.](#)

[Figure 7.18 Standing exercise - bend over.](#)

[Figure 7.19 Standing exercise - reach up.](#)

[Figure 7.20 Standing exercise - turn 180°.](#)

[Figure 7.21 Walking exercise - looking at the horizon.](#)

[Figure 7.22 Walking exercise - yaw.](#)

[Figure 7.23 Walking exercise - pitch.](#)

[Figure 7.24 Avatar following the index finger with the eyes.](#)

[Figure 7.25 Opened eyes.](#)

[Figure 7.26 Closed eyes.](#)

[Figure 7.27 Speech recognition workflow.](#)

[Figure 7.28 Motion tracking - marker-less based system.](#)

[Figure 7.29 Motion tracking - marker-based system.](#)

[Figure 7.30 Motion capture professional studio.](#)

[Figure 7.31 HOLOBALANCE target image.](#)

[Figure 7.32 Unity's Avatar structure.](#)

[Figure 7.33 Animation using a muscle-based control framework.](#)

[Figure 7.34 A biomechanical upper limb model. On the left, the elbow is actu...](#)

[Figure 7.35 Inverse dynamics-based optimization. The optimization problem it...](#)

[Figure 7.36 Forward dynamics-based optimization. The optimization problem it...](#)

[Figure 7.37 Tension-velocity curve corresponding to a muscle in the tetanize...](#)

[Figure 7.38 Isometric tension-length curve.](#)

[Figure 7.39 Hill's functional model of a muscle. CE is the contractile eleme...](#)

Chapter 8

[Figure 8.1 Heart geometry and seven different regions of the model: \(1\) Sino...](#)

[Figure 8.2 Six electrodes \(V1-V6\) positioned at the chest to model the preco...](#)

[Figure 8.3 Material local coordinate system according to \[14\]. Biaxial loadi...](#)

[Figure 8.4 Experimental curves with hysteresis for biaxial loading of myocar...](#)

[Figure 8.5 Experimental curves without hysteresis for biaxial loading of myo...](#)

[Figure 8.6 Interpolation of normal stresses in the local \(material\) coordina...](#)

[Figure 8.7 Shear stresses acting on material element.](#)

[Figure 8.8 Shear stresses in terms of shear deformation for three modes. \(a\)...](#)

[Figure 8.9 Shear stress constitutive curves, no hysteresis \(Figure 8.13 \[14\]...](#)

[Figure 8.10 Whole heart activation simulation from lead II ECG signal at var...](#)

[Figure 8.11 Simulated and measured ECG for six electrodes \(V1-V6\).](#)

[Figure 8.12 Body surface potential maps in a healthy subject during progress...](#)

[Figure 8.13 Model of the human heart: \(a\) Purkinje network; \(b\) uniform Purk...](#)

Chapter 9

[Figure 9.1 Design flow of Xilinx System Generator use in implementing an alg...](#)

[Figure 9.2 Xilinx System Generator library.](#)

[Figure 9.3 Schematic icons for some of the widely used XSG elements. \(a\) Xil...](#)

[Figure 9.4 Image preprocessing module.](#)

[Figure 9.5 Image post-processing module.](#)

[Figure 9.6 Simulink - System Generator DSP model for creating negative image...](#)

[Figure 9.7 Simulink - System Generator DSP model for image contrast stretchi...](#)

[Figure 9.8 Robert method - System Generator DSP sub-model for horizontal mas...](#)

[Figure 9.9 Robert method - System Generator DSP sub-model for vertical mask ...](#)

[Figure 9.10 Prewitt method - System Generator DSP sub-model for horizontal m...](#)

[Figure 9.11 Prewitt method - System Generator DSP sub-model for vertical mas...](#)

[Figure 9.12 Sobel method - System Generator DSP sub-model for horizontal mas...](#)

[Figure 9.13 Sobel method - System Generator DSP sub-model for vertical mask ...](#)

[Figure 9.14 System Generator DSP sub-model for thresholding method.](#)

[Figure 9.15 System Generator DSP model for Canny Edge detection.](#)

[Figure 9.16 Canny method - System Generator DSP sub-model for Gaussian smoot...](#)

[Figure 9.17 Canny method - System Generator DSP sub-model for edge detection...](#)

[Figure 9.18 Canny method - System Generator DSP sub-model for Non-Maximum Su...](#)

[Figure 9.19 Canny method - System Generator DSP sub-model for Hysteresis thr...](#)

[Figure 9.20 Combined software and hardware co-simulation model for the edge ...](#)

[Figure 9.21 Original and output image after application of algorithm for ima...](#)

[Figure 9.22 Original and output image after application of algorithm for con...](#)

[Figure 9.23 Original image \(a\) compared with output images after application...](#)

Figure 9.24 Canny edge detection sub-steps:
Gaussian smoothing_(a), calculat...

IEEE Press
445 Hoes Lane
Piscataway, NJ 08854

IEEE Press Editorial Board
Ekram Hossain, *Editor in Chief*

Jón Atli Benediktsson	Xiaoou Li	Jeffrey Reed
Anjan Bose	Lian Yong	Diomidis Spinellis
David Alan Grier	Andreas Molisch	Sarah Spurgeon
Elya B. Joffe	Saeid Nahavandi	Ahmet Murat Tekalp

Computational Modeling and Simulation Examples in Bioengineering

Edited by

Nenad D. Filipovic
Faculty of Engineering
University of Kragujevac
SERBIA



IEEE Engineering in Medicine
and Biology Society, *Sponsor*



IEEE Press Series in Biomedical Engineering
Metin Akay, *Series Editor*



IEEE PRESS
WILEY

The IEEE Press logo consists of a stylized sunburst or fan shape above the text 'IEEE PRESS'. Below this, the word 'WILEY' is printed in a large, bold, serif font.

Copyright © 2022 by The Institute of Electrical and Electronics Engineers, Inc.
All rights reserved.

Published by John Wiley & Sons, Inc., Hoboken, New Jersey.
Published simultaneously in Canada.

No part of this publication may be reproduced, stored in a retrieval system, or transmitted in any form or by any means, electronic, mechanical, photocopying, recording, scanning, or otherwise, except as permitted under Section 107 or 108 of the 1976 United States Copyright Act, without either the prior written permission of the Publisher, or authorization through payment of the appropriate per-copy fee to the Copyright Clearance Center, Inc., 222 Rosewood Drive, Danvers, MA 01923, (978) 750-8400, fax (978) 750-4470, or on the web at www.copyright.com. Requests to the Publisher for permission should be addressed to the Permissions Department, John Wiley & Sons, Inc., 111 River Street, Hoboken, NJ 07030, (201) 748-6011, fax (201) 748-6008, or online at <http://www.wiley.com/go/permission>.

Limit of Liability/Disclaimer of Warranty: While the publisher and author have used their best efforts in preparing this book, they make no representations or warranties with respect to the accuracy or completeness of the contents of this book and specifically disclaim any implied warranties of merchantability or fitness for a particular purpose. No warranty may be created or extended by sales representatives or written sales materials. The advice and strategies contained herein may not be suitable for your situation. You should consult with a professional where appropriate. Neither the publisher nor author shall be liable for any loss of profit or any other commercial damages, including but not limited to special, incidental, consequential, or other damages.

For general information on our other products and services or for technical support, please contact our Customer Care Department within the United States at (800) 762-2974, outside the United States at (317) 572-3993 or fax (317) 572-4002.

Wiley also publishes its books in a variety of electronic formats. Some content that appears in print may not be available in electronic formats. For more information about Wiley products, visit our web site at www.wiley.com.

Library of Congress Cataloging-in-Publication Data

Names: Filipovic, Nenad, D., editor.

Title: Computational modeling and simulation examples in bioengineering / edited by Nenad D. Filipovic, Faculty of Engineering, University of Kragujevac, Serbia.

Description: First edition. | Hoboken, New Jersey : Wiley, [2022] | Series: IEEE press series on biomedical engineering | Includes index.

Identifiers: LCCN 2021039449 (print) | LCCN 2021039450 (ebook) | ISBN 9781119563945 (hardback) | ISBN 9781119563921 (adobe pdf) | ISBN 9781119563914 (epub)

Subjects: LCSH: Biomedical engineering. | Computer simulation.

Classification: LCC R856 .C626 2022 (print) | LCC R856 (ebook) | DDC 610.28-

dc23/eng/20211005

LC record available at <https://lccn.loc.gov/2021039449>

LC ebook record available at <https://lccn.loc.gov/2021039450>

Cover Design: Wiley

Cover Image: © archy13/Shutterstock

Editor Biography



Nenad D. Filipovic is Rector of University of Kragujevac, Serbia, full Professor at Faculty of Engineering and Head of Center for Bioengineering at University of Kragujevac, Serbia. He was Research Associate at Harvard School of Public Health in Boston, USA. His research interests are in the area of biomedical engineering, cardiovascular disease, fluid-structure interaction, biomechanics, bioinformatics, biomedical image processing, machine learning, medical informatics, multi-scale modeling, software engineering, parallel computing, computational chemistry, and bioprocess modeling. He is author and coauthor of 11 books, over 350 publications in peer-reviewed journals, and over 10 software for modeling with finite element method and discrete methods from fluid mechanics and multiphysics. He also leads a number of national and international projects in the EU and United States in the area of bioengineering and software development.

He is Director of Center for Bioengineering at University of Kragujevac and leads joint research projects with Harvard University and University of Texas in the area of bio-nanomedicine computer simulation. He also leads a number of national and international projects in the area of bioengineering and bioinformatics. He is Editor in Chief for EAI Endorsed Transaction on Bioengineering and Bioinformatics, Managing Editor for Journal of Serbian Society for Computational Mechanics, President of Serbian Society of Mechanics and member of European Society of Biomechanics (ESB), European Society for Artificial Organs (ESAO), and IEEE member.

Author Biographies

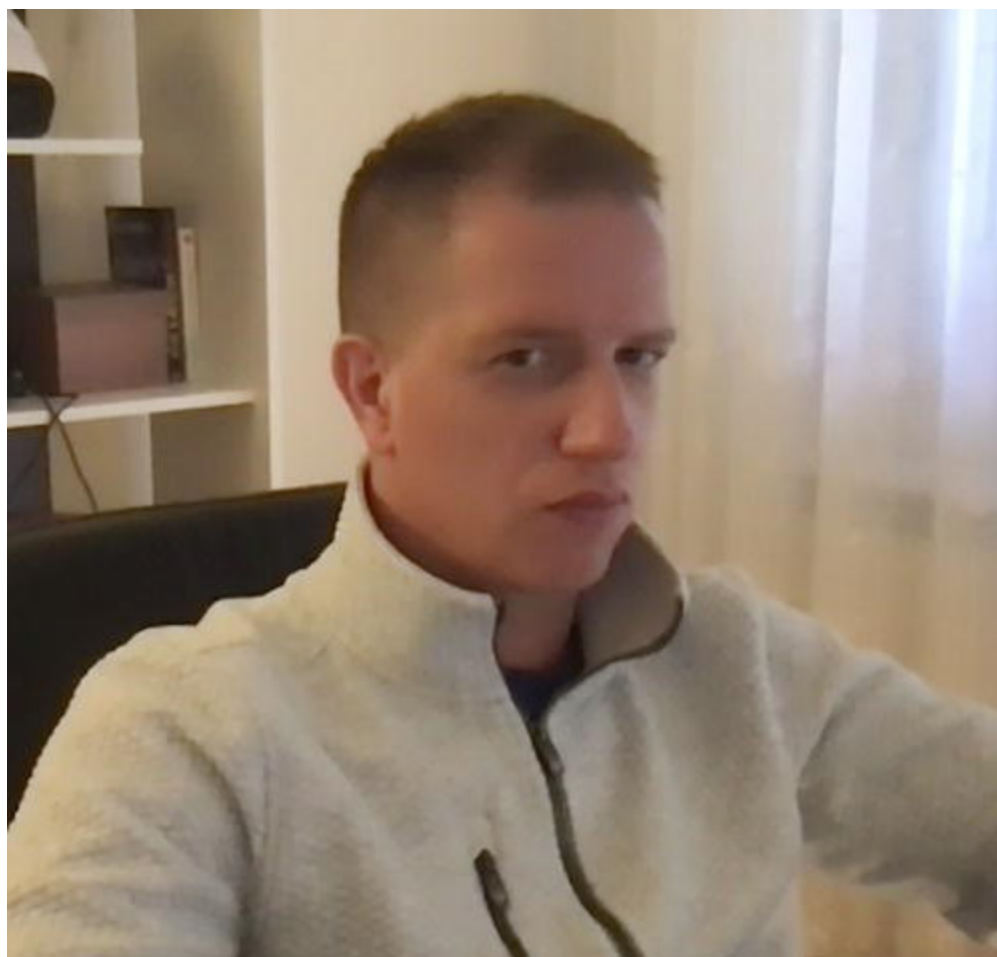


Tijana Djukic (born on 1st April 1988) is a PhD in biomedical engineering. She finished Bachelor and Master studies at Faculty of Mechanical Engineering, University of Kragujevac, Serbia, with average mark 10. She finished

PhD studies at the same faculty, with average mark 10 in 2015, for a record period of less than three years. Currently, she works as a Senior Research Associate at Institute for Information Technologies, University of Kragujevac, Serbia, and is involved in projects regarding software development of applications in bioengineering. Her main research interests are in the area of computational mechanics, solid-fluid interaction, microfluidics, multi-scale cancer modeling, parallel computing using GPU devices, and modeling using finite element and lattice Boltzmann method. She speaks English, German, and Spanish, and uses Italian and French.



Ksenija Zelic Mihajlovic is a Doctor of Dental Medicine, PhD in dental sciences, and a specialist in Periodontology and Oral Medicine with more than 12 years of clinical practice. She holds the position of a Research Associate at the School of Dentistry, University of Belgrade, Serbia, and has published 24 scientific papers in prestigious international peer-reviewed journals with more than 400 citations. Focus of her basic and clinical research for 12 years has been on nanostructure of dental tissues, nanotechnology, computational modeling and biomechanics in dental sciences and practice, forensic dentistry, periodontology, and endodontics.



Zarko Milosevic was born on 14 March 1983. He received his Master's degree from Faculty of Mechanical Engineering University of Kragujevac in 2009 and his PhD